



Defects modified in the exfoliation of $g\text{-C}_3\text{N}_4$ nanosheets via a self-assembly process for improved hydrogen evolution performance

Jian Wang^{a,b}, Zhuang Yang^{a,b}, Wenqing Yao^{b,*}, Xingxing Gao^c, Dongping Tao^a

^a School of Mining Engineering, University of Science and Technology Liaoning, Anshan 114051, Liaoning province, PR China

^b Department of Chemistry, Tsinghua University, Beijing 100084, PR China

^c School of Civil engineering, University of Science and Technology Liaoning, Anshan 114051, Liaoning province, PR China



ARTICLE INFO

Keywords:

Carbon nitride
Modifying defects
Self-assembly process
Hydrogen evolution performance

ABSTRACT

In this work, self-assembly $g\text{-C}_3\text{N}_4$ samples were prepared without templates by a facile method involving thermal oxidation etching of bulk $g\text{-C}_3\text{N}_4$ and subsequent reflux in the different organic solvent at a low temperature. The internal hydrogen bond, cyano and amino defects of $g\text{-C}_3\text{N}_4$ nanosheets can be partly repaired via refluxing in the different polarity of the organic solvent, which is attributed to the effect of hydrogen bond polarity, hydroxyl and carbon chain structure of organic solvent. Especially, refluxing in the solvent of isopropanol, $g\text{-C}_3\text{N}_4$ nanosheets have transformed into quasi-sphere structure via a self-assembly process utilizing the effect of Oswald, which evidently reduced defect density within a molecular of $g\text{-C}_3\text{N}_4$, because of strong interaction between the generation of C–O bond of $g\text{-C}_3\text{N}_4$ nanosheets during refluxing in the isopropanol solvent and molecular group of isopropanol (hydroxyl group and the carbon chain structure). The self-assembly quasi-sphere $g\text{-C}_3\text{N}_4$ samples exhibit much faster photocatalytic hydrogen evolution rate than other $g\text{-C}_3\text{N}_4$ samples under visible light irradiation and the hydrogen evolution rate is $30.67\text{ }\mu\text{mol h}^{-1}$, which is about 10 times higher than that of bulk $g\text{-C}_3\text{N}_4$. The enhanced hydrogen evolution performance for quasi-sphere $g\text{-C}_3\text{N}_4$ samples is ascribed to large surface areas and accelerated separation of charges.

1. Introduction

The increasing issue of environmental pollution and energy shortage has become a serious challenge stimulating the research on low-cost, high-efficiency and environment friendly energy systems [1–4]. Semiconductor photocatalytic method has received persistent interest for its applications in solar energy conversion and pollutants decomposition [5–8]. In recent years, a significant number of semiconductor materials have been proffered as photocatalyst for production of H_2 and degradation of organic pollutants [9,10]. Among them, graphitic carbon nitride ($g\text{-C}_3\text{N}_4$) as a novel metal-free photocatalyst with a bandgap of 2.7 eV [11] and conjugated π system has drawn widely attention due to its transcendent characters such as easy availability [12–15], high stability [16–18] and optical properties [19–23]. Owing to its activity under visible light, $g\text{-C}_3\text{N}_4$ has been investigated as photocatalysts for applications of water splitting and environmental purification. Bulk $g\text{-C}_3\text{N}_4$ can be easily available via calcining the precursors such as melamine [24], dicyandiamide [25,26] and urea [27]. However, bulk $g\text{-C}_3\text{N}_4$ gained by the aforesaid method directly suffers from the shortcomings such as small specific surface area [28–30], low

quantum efficiency [31–33] and high electron-hole recombination [24,34,35], induce that its application in many areas has been limited. Like other photocatalyst materials, a variety of approaches including heteroatom introducing [6,36–38], semiconductor compositing [39–41] and morphology changing [14,42,43] have been employed to enhance the photocatalytic activity of bulk $g\text{-C}_3\text{N}_4$.

As we all know, the morphology, size and specific surface area of materials all have a great influence on photocatalytic activity of nanostructures [41]. Unfortunately, the specific surface areas of bulk $g\text{-C}_3\text{N}_4$ are not adequate for performing its activities. Two-dimensional (2D) nanomaterials have attracted tremendous attention in virtue of their extraordinary atomic-layer thickness which can promote the photoresponse [44]. Owing to the laminated structure composed of tri-s-triazine units and triazine units (Fig. S1), bulk $g\text{-C}_3\text{N}_4$ possess a weak van der Waals force between C–N layers [45,46], so that $g\text{-C}_3\text{N}_4$ nanosheets, which can result in enhanced photoresponsivity, should be available via exfoliation process. In order to obtain the 2D nanostructure, a series of approaches switching bulk $g\text{-C}_3\text{N}_4$ to nanosheets for heightening photocatalytic activities of $g\text{-C}_3\text{N}_4$ have been reported in succession. For example, Niu et al. prepared $g\text{-C}_3\text{N}_4$ nanosheets via

* Corresponding author.

E-mail address: yaowq@mail.tsinghua.edu.cn (W. Yao).

thermal oxidation “etching” method in air [37]. The nanosheets exhibit average hydrogen evolution rate 5.4 and 3 times compared with the bulk g-C₃N₄ under UV-vis and visible light respectively. Bai et al. obtained g-C₃N₄ nanosheets via tailoring bulk g-C₃N₄ using chemical scissors composed by NH₃ and H₂O₂ [47]. The charge separation process has been improved by the new structures leading to photocatalytic activity has been enhanced in hydrogen production. Zhang et al. prepared g-C₃N₄ nonasheets via liquid exfoliation in water [48]. The ultrathin nanosheets performance enhanced photoabsorption and photoresponse. Huang et al. synthesized g-C₃N₄ nonasheets via ultrasonic exfoliation and the g-C₃N₄ nonasheets show larger specific surface area, higher photocurrent response and higher photocatalytic activity than bulk g-C₃N₄ [49]. Xu et al. reported that Nano-size g-C₃N₄ prepared by HNO₃ modification and calcination possesses a large specific surface area and its photoactivity in degrading Methyl Orange under visible-light irradiation has been enhanced [50]. However, the exposure of defects-relatively low crystallinity due to incomplete polymerization which lead to the formation of medium strong planar hydrogen bonds during the condensation process [45] are unavoidable during the synthesis [51], and little data about elimination of the hydrogen bonds defects, especially via a second calcination and self-assembly process for enhancing crystalline of graphitic carbon nitride, could be available from preventient studies.

Although it's found that exfoliated g-C₃N₄ nanosheets possess more photocatalytic activity, to the best of our knowledge, few attempts have been made on the relationship between g-C₃N₄ morphologies and solvent varieties during the synthesis of elimination of the hydrogen bonds and structure defects of g-C₃N₄ nanosheets after exfoliation, especially the self-assembly of nanosheets which transform to spheres configuration. In this work, we synthesized the self-assembly g-C₃N₄ samples without templates, the internal hydrogen bond, cyano and amino defect density of which have been reduced via the modified process with a simple refluxed method. The ultrapure water, methanol, ethanol and isopropanol were used as solvents for the morphology reforming, and the hydrogen bond polarity, hydroxyl and carbon chain structure have been explored. All the self-assembly g-C₃N₄ samples, especially the samples synthesized in isopropanol solvent, have a high photocatalytic activity for visible-light hydrogen evolution. Herein, the morphology, structure and optical property of synthesized g-C₃N₄ samples have been characterized. The possible exfoliation and self-assembly mechanism and the enhanced visible-light photocatalytic activity mechanism have been studied.

2. Experimental

All the chemicals utilized in this research were of analytical-grade without further purification.

2.1. Preparation of different g-C₃N₄ photocatalysts

Typically, 5 g of melamine (C₃H₆N₆) in a covered crucible was heated to 550 °C held for 4 h with a ramping rate of 2 °C/min in a muffle furnace. The product was ground into yellow powder in a mortar and then heated to 500 °C held for 2 h with a ramping rate of 5 °C/min in an opened crucible. About 1 g of the product after the second calcine was put into 200 ml of ultrapure water followed by ultrasonic exfoliation for 8 h. Deposited for overnight, the suspension was centrifuged and dried and then the g-C₃N₄ nanosheets were obtained for further use.

About 0.1 g of the g-C₃N₄ nanosheets were added into 100 ml of ultrapure water, methanol, ethanol and isopropanol respectively. After being stirred vigorously, the solution was transferred into a 250 ml round-bottom flask and refluxed at 65 °C for 12 h, and then allowed to cool naturally to room temperature. Subsequently, the photocatalysts can be obtained after the evaporation of solvent and the resulting samples were washed with ultrapure water for three times under centrifugation in 7000 rpm. The products synthesized in ultrapure water,

methanol, ethanol and isopropanol were named as C₃N₄-water, C₃N₄-methanol, C₃N₄-ethanol and C₃N₄-isopropanol respectively. The C₃N₄ yield is 93.4%, 93.2%, 92.9% and 93.3% for C₃N₄-water, C₃N₄-methanol, C₃N₄-ethanol and C₃N₄-isopropanol respectively.

2.2. Characterization of different g-C₃N₄ photocatalysts

The crystal structure of the powders was analyzed via X-ray diffraction (XRD) on a Rigaku D/max-2400 X-ray diffractometer with CuK α irradiation (40 kV, 20 mA; $\lambda = 1.5406 \text{ \AA}$). The morphology of the products was observed by a scanning electron microscope (SEM, Hitachi S-3500 N) and a transmission electron microscope (TEM, JEOL JEM2011 F). The UV-vis absorption spectra of the samples was obtained on a UV-vis spectrophotometer (Hitachi UV-3010), and BaSO₄ was used as a reference. Fourier transform infrared (FT-IR) spectra were recorded on a Bruker VERTEX-70 spectrometer. X-ray photoelectron spectroscopy (XPS) measurements were recorded on PHI Quantera SXM with a monochromatized Al Ka X-ray source (pass energy 55 eV). The Brunauer-Emmett-Teller (BET) specific surface area and the pore distribution of the samples were evaluated by N₂ adsorption/desorption using Micromeritics ASAP2010 V5.02H. The photoluminescence (PL) spectra of the samples were obtained via on LS55 fluorescence spectrometer (Perkin-Elmer, USA) with an excitation wavelength of 370 nm at room temperature. The photocurrents and electrochemical impedance spectroscopy (EIS) were measured on an CHI 660B electrochemical system. Electron spin resonance (EPR) measurements were recorded on MiniScope MS5000 EPR spectrometer.

2.3. Photocatalysis experiments

Photocatalytic H₂ generation under visible-light irradiation which was implemented by a 300 W Xe lamp with a 420 nm cutoff filter was selected to evaluate the photocatalytic activity of the samples. The reactions were carried out in a closed Pyrex top-irradiation reaction vessel with a glass closed gas system. Typically, 50 mg of catalyst powder was dispersed in 100 ml of aqueous solution containing 20 vol. % triethanolamine (TEOA). 3 Wt % Pt was loaded on the surface of catalyst via an in site photodeposition method with H₂PtCl₆. The reaction solution was purged with argon for 30 min to remove the residual air in the reactor. The flow of cooling water was used to maintain the room temperature of the reactor. The evolved gas products were analyzed via a gas chromatography with a thermal conductive detector (TCD). For a stability test, C₃N₄ samples was used to catalyze the photocatalytic hydrogen evolution for the first 4 h using the method mentioned above. Then, the reaction system was vacuumized 4 h to remove the generated H₂ gas completely. After that, the photocatalytic reaction was continued for another 4 h. The whole reaction was circulated five circles (i.e., a 20 h recycling experiment with intermittent evacuation every 4 h).

2.4. Electrochemical measurement

The photocurrent and electrochemical impedance spectroscopy (EIS) tests were performed on the electrochemical workstation (CHI 660E, China) using tripolar systems under visible light irradiation. The indium-tin oxide (ITO) glass loading catalyst is used as the working electrode, saturated calomel and platinum wire were used as reference electrode and counter electrode, respectively. Na₂SO₄ solution with a concentration of 0.1 M is used as the electrode solution.

Membrane electrode was prepared via drip coated method: 10 mg photocatalyst was ultrasonic dispersed into 1 ml of ethanol, dripping solution coated on 2 cm × 4 cm ITO glass evenly and deposited for overnight. The membrane electrode was calcined at 150°C for 2 h, and then cooled to room temperature slowly. The bias voltage of the photocurrent response is 0 V, and the EIS is carried out in the open circuit with a frequency of 0.01–10000 Hz.

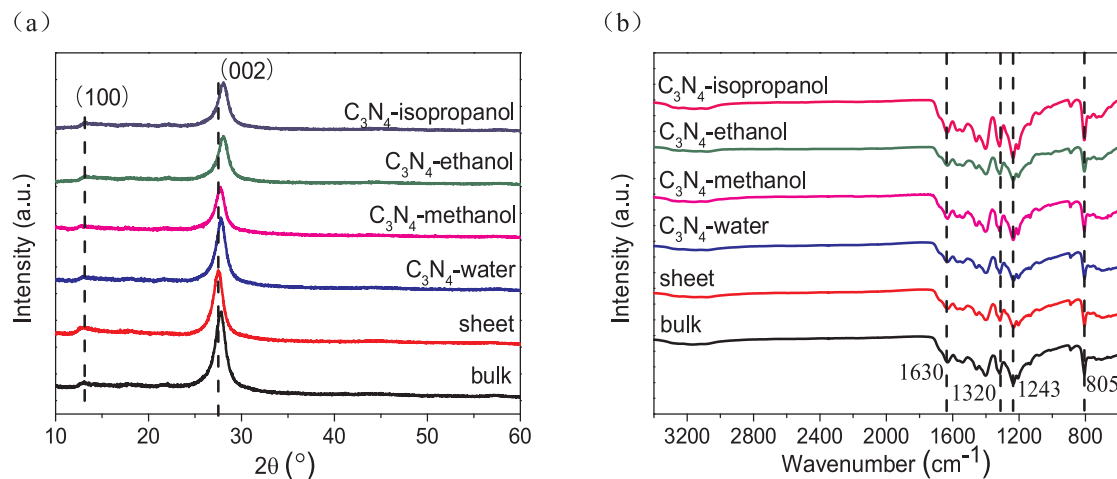


Fig. 1. (a) XRD patterns. (b) FTIR spectra. of bulk g-C₃N₄, nanosheets and the refluxed samples in different solvent systems.

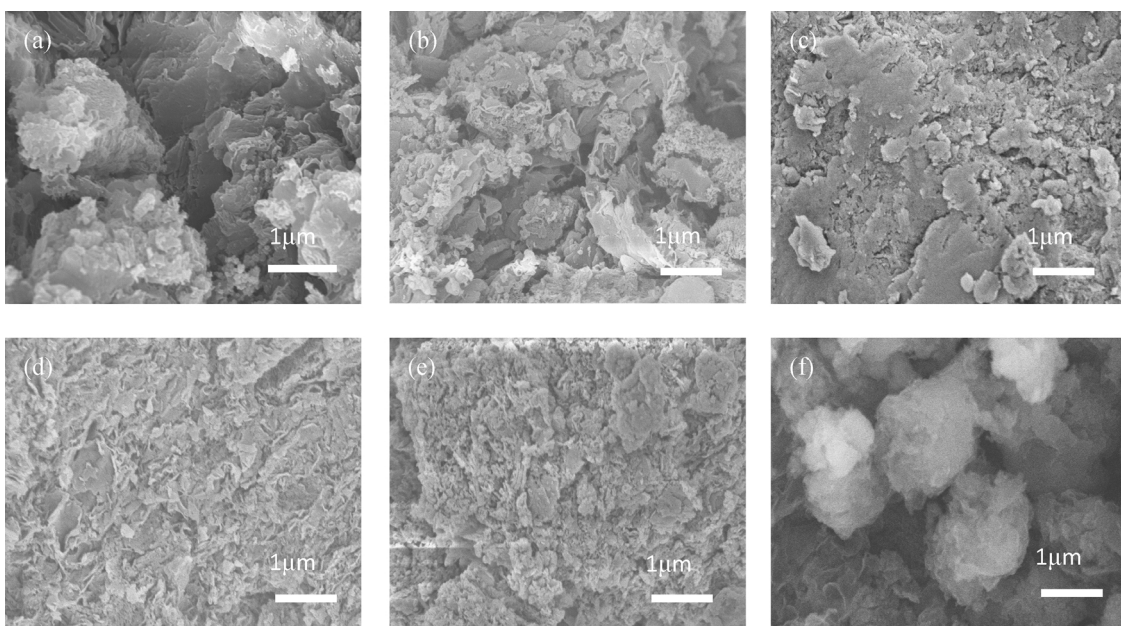


Fig. 2. SEM images of (a) bulk, (b) sheet, (c) C₃N₄-water, (d) C₃N₄-methanol, (e) C₃N₄-ethanol, (f) C₃N₄-isopropanol samples.

Table 1
Characterization results of as-prepared samples.

Sample	bulk	C ₃ N ₄ -water	C ₃ N ₄ -methanol	C ₃ N ₄ -ethanol	C ₃ N ₄ -isopropanol
Absorption edge/nm	463	466	455	454	457
Band gap/eV	2.70	2.62	2.71	2.72	2.66
CB/eV	-1.30	-1.36	-1.42	-1.43	-1.47
VB/eV	+1.40	+1.26	+1.29	+1.29	+1.19
morphology	bulk	aggregated sheets	aggregated sheets	aggregated sheets	spheres
Surface area / m ² g ⁻¹	24.95	43.16	85.97	94.68	155.88
IPCE / %	1.41	1.81	2.12	2.18	3.02
HER / $\mu\text{mol}\cdot\text{h}^{-1}$	3.03	7.67	12.87	14.17	30.67

3. Results and discussion

3.1. The structure of high specific surface area

The phase composition and crystallite dimension of as-prepared samples were analyzed via X-ray diffraction (XRD) patterns. According to the reports before [52], the XRD diffraction characteristic peaks of pure g-C₃N₄ appear at 2θ = 13.1° and 27.4°, corresponding to (100) and (002) crystal plane of graphitic structure. As shown in Fig. 1a, all the samples showed XRD diffraction characteristic peak, and no other miscellaneous peaks appeared, indicating the crystal structure characteristics were retained after the exfoliation and assembly process. The strong peak at 27.4° belong to the aromatic ring system stack peak, and the position of (002) crystal plane for g-C₃N₄ nanosheets is slightly smaller than that of bulk g-C₃N₄, indicating the space of the crystal surface increased, and the bulk g-C₃N₄ changed into laminated structure successfully. Compared with g-C₃N₄ nanosheets, the (002) crystal planes of self-assembly samples moved to the right slightly, illustrating the space of the crystal surface decreased, due to the refluxed process increased the degree of stack of aromatic ring system. The (100) crystal planes of the refluxed samples which according to the conjugate length

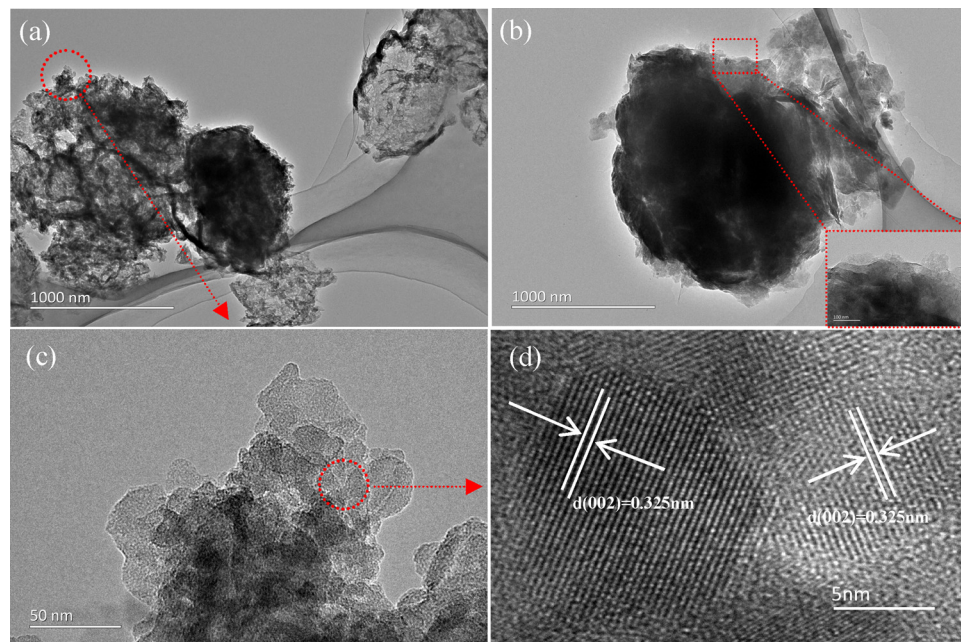


Fig. 3. TEM measurements of C_3N_4 -isopropanol samples. (a,b) low-magnification TEM images clearly showing that C_3N_4 -isopropanol samples have quasi-sphere morphology with diameters of approximate 0.8–1.2 μm . (c) High magnification TEM image of C_3N_4 -isopropanol samples. (d) HRTEM image of C_3N_4 -isopropanol samples showing its lattice planes.

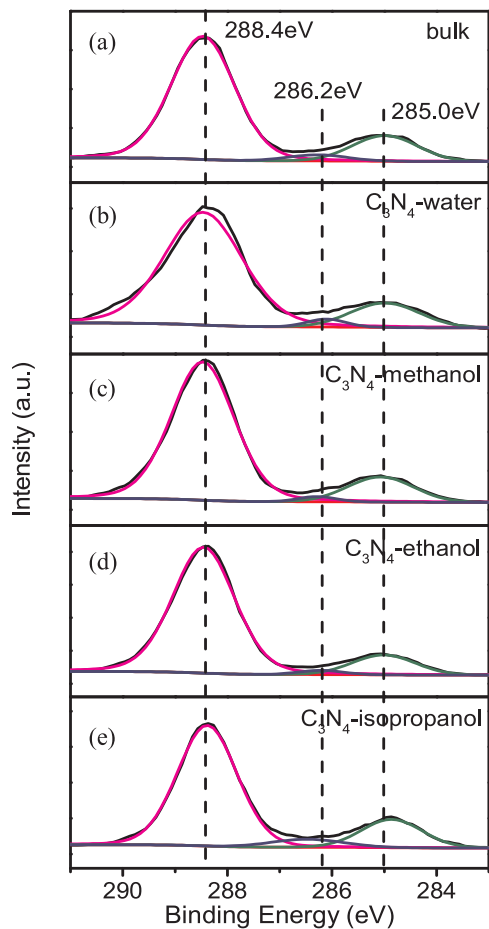


Fig. 4. C1s XPS spectra of as-prepared samples.

of the repeated structure were reduced, indicating the crystal planes changed from the long range to the near order. The (100) diffraction peak of $\text{g-C}_3\text{N}_4$ nanosheets should have disappeared, however, there was a stronger signal, indicating the interaction the van der Waals force during the drying process. In order to further determine the structure of

as-prepared samples, FTIR spectra was used to characterize the samples. As shown in Fig. 1b, the FTIR spectra proves that the basic structure of the samples have not changed obviously. The peaks located at 805 cm^{-1} are ascribed to the s-triazine ring system of the $\text{g-C}_3\text{N}_4$. The $1200\text{--}1650\text{ cm}^{-1}$ region corresponds to the typical C–N heterocyclic stretching vibration, the absorption of 3000 to 3400 cm^{-1} are possibly corresponding to N–H and N–H₂ of the breakage edge of the aromatic ring and the adsorption of water molecules in the air.

The morphology and microstructure of the as-prepared samples were investigated via SEM and TEM images. As a comparison, the SEM image of bulk- C_3N_4 , C_3N_4 nanosheets and refluxed samples in the different organic solvent are shown in Fig. 2. It can be seen that C_3N_4 -water, C_3N_4 -methanol and C_3N_4 -ethanol samples maintain uneven aggregated sheets structure (Fig. S2 for TEM images), however, it is worth noting that C_3N_4 -isopropanol samples have self-assembled into quasi-sphere morphology, and the average diameter of which is about 1 μm . Compared with other morphology, the quasi-sphere structure of C_3N_4 -isopropanol possess a large specific surface area, which is about 6.25 times that of bulk $\text{g-C}_3\text{N}_4$ (Table 1). Fig. S3 shows the N_2 adsorption-desorption curves. The incompact and multi-hole structure of C_3N_4 -isopropanol samples can provide more active sites which can promote the photocatalysts efficiency. The TEM images in Fig. 3 further confirmed the well-defined quasi-sphere structure of C_3N_4 -isopropanol samples. As shown in Fig. 3a, low magnification TEM image exhibit that all C_3N_4 -isopropanol samples were quasi-sphere morphology and good mono-dispersivity. Fig. 3b clearly displays that the monodisperse C_3N_4 -isopropanol particle has a diameter of 1.2 μm , well in agreement with SEM images. Local high-magnification TEM image reveal that C_3N_4 nanosheets layer by layer self-assembled into the final quasi-sphere structure (inset of Fig. 3b and Fig. 3c). High-resolution TEM (HRTEM) image of the C_3N_4 -isopropanol samples in Fig. 3d shows that the lattice plane separation of C_3N_4 -isopropanol is about 0.325 nm, corresponding to the (002) crystal plane of graphitic structure, which is consistent with the XRD result.

X-ray photoelectron spectroscopy (XPS) was used to further investigate the chemical states of as-prepared samples. Fig. 4 shows the C1s peaks, three peaks of C_3N_4 -isopropanol at 288.4 eV, 285.0 eV and > 286.0 eV were observed in the C1s XPS spectrum. The peaks at 288.4 eV were attribute to sp^2 -hybridized carbon (N–C=N), which are in the N-containing aromatic ring and considered as the main aromatic carbon species for the framework. The peaks at 285.0 eV were attribute

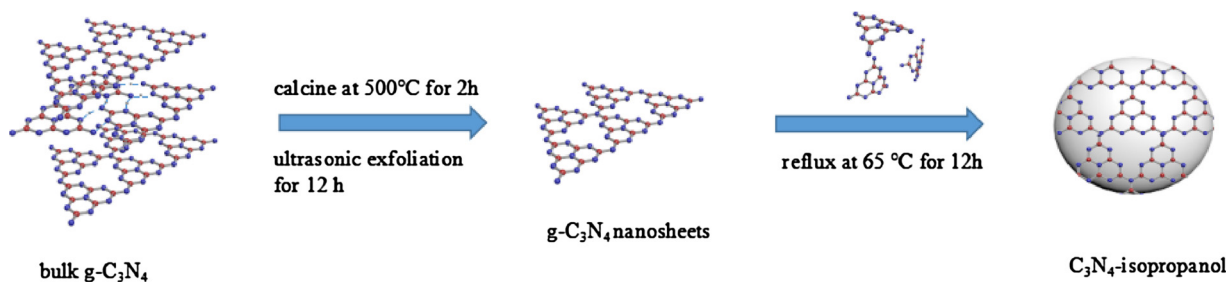


Fig. 5. Schematic illustration of self-assembly mechanism for C_3N_4 -isopropanol samples.

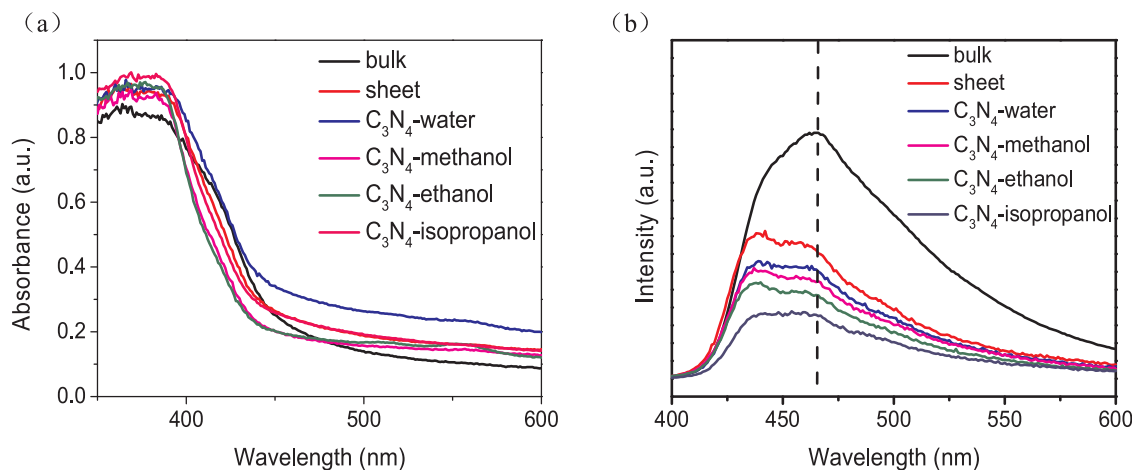


Fig. 6. (a) UV-vis diffuse reflection spectra. (b) Photoluminescence spectra (excited at 370 nm) of bulk $\text{g-C}_3\text{N}_4$, nanosheets and the refluxed samples in different solvent systems.

to carbon (C–C). The weak peaks at > 286.0 eV may be explained as follows: as shown in Fig. 4a–d, The 286.2 eV peaks of the as-prepared samples are assigned to a small quantity of carbon combined of C–N. The 286.5 eV peak of C_3N_4 -isopropanol sample is most different with other samples, as shown in Fig. 4e, the peak possesses a wider half peak width and a larger peak area, which can be attributable to the carbon combined of (C–O–C) or (C–O–H). It may be that the symmetric branched chain structure of isopropanol is different from other solvents, resulting in a small amount of (C–O) bonding. The nanosheets are more likely to pile up, due to the unique symmetry of solvent and the (C–O) bond, resulting in the C_3N_4 -isopropanol sample transform to the sphere with a large volume and a higher surface area, and this result is consistent with SEM.

Based on the aforesaid result and analysis, we can come to a conclusion that quasi-sphere C_3N_4 samples may have experienced a self-assembly process involving exfoliation and regrowth in the solvent of isopropanol (Fig. 5). The formation mechanism of regenerative $\text{g-C}_3\text{N}_4$ can be summarized as follows: (1) Bulk $\text{g-C}_3\text{N}_4$ undergo a twice calcination to form the high polymerization $\text{g-C}_3\text{N}_4$ and a ultrasonic treatment in the medium ultrapure water, and then the lamellar structure $\text{g-C}_3\text{N}_4$ nanosheets were obtained by this method. The synthesis of $\text{g-C}_3\text{N}_4$ nanosheets is a fundamental step of the formation of reborn $\text{g-C}_3\text{N}_4$ nanostructure, since the hydrogen-bond defects mentioned before have been decreased and the lamellar structure is essential to self-assembly. (2) In the refluxing system, the (C–O) of nanosheets bonded by the hydroxyl group and the carbon chain structure, and the cyanogen and amino defects of the internal structure are repaired. The layer structure $\text{g-C}_3\text{N}_4$ nanosheets were in a metastable state and tend to incurvate, which could result in their accumulation and the quasi-sphere structure may appear during the reflux treatment. (3) During the residual reflux process, the layer structure $\text{g-C}_3\text{N}_4$ nanosheets continue to roll onto the surface of sphere to form a stable and fleecy structure. The structure of the final sample may depend on the polar molecules of

the medium containing hydroxyl structure. When nanosheets regrow in isopropanol solvent, (C–O–C) or (C–O–H) structure has formed influenced by the hydroxyl and symmetric branched chain, and lamella structure increase the degree and rate of bonding and crimp, leading to the heptyl oxazine ring is more likely to stack.

3.2. Separation of charge under visible light

UV-vis absorption spectra of as-prepared samples are shown in Fig. 6a. All the as-prepared samples exhibit typical and strong UV-vis absorption characteristics, and the absorption edge of bulk $\text{g-C}_3\text{N}_4$ is about 460 nm. It can be seen the absorption edge of C_3N_4 -methanol, C_3N_4 -ethanol, C_3N_4 -isopropanol show a slight blue shift with respect to bulk $\text{g-C}_3\text{N}_4$, which can be attributed to the quantum confinement effect, and this result is consistent with the phenomenon that the colour of the samples changed from yellow to white. The light absorption of the samples is enhanced in the visible light region, indicating that more charge carriers could be generated with visible-light irradiation. The corresponding band gap of the as-prepared samples are shown in Table 1. The separation / recombination of charge carries and the reduced density of structural defects can be determined via the photoluminescence spectra (PL). As illustrated in Fig. 6b, the major emission wavelength of the refluxed samples show a slight blue-shift in comparison to bulk $\text{g-C}_3\text{N}_4$, which can be also attributed to the quantum confinement effect, and this is consistent with the UV-vis absorption spectra result. In addition, the PL intensity for C_3N_4 -isopropanol decreased significantly compared with bulk $\text{g-C}_3\text{N}_4$, and the intensities of the pattern are in order of bulk $>$ sheets $>$ C_3N_4 -water $>$ C_3N_4 -methanol $>$ C_3N_4 -ethanol $>$ C_3N_4 -isopropanol. The PL intensity of the treated samples decreased significantly, indicating that the separation efficiency of photogenerated charge carries was obviously improved, and the defect density of the internal structure as the electron-hole composite center decreased.

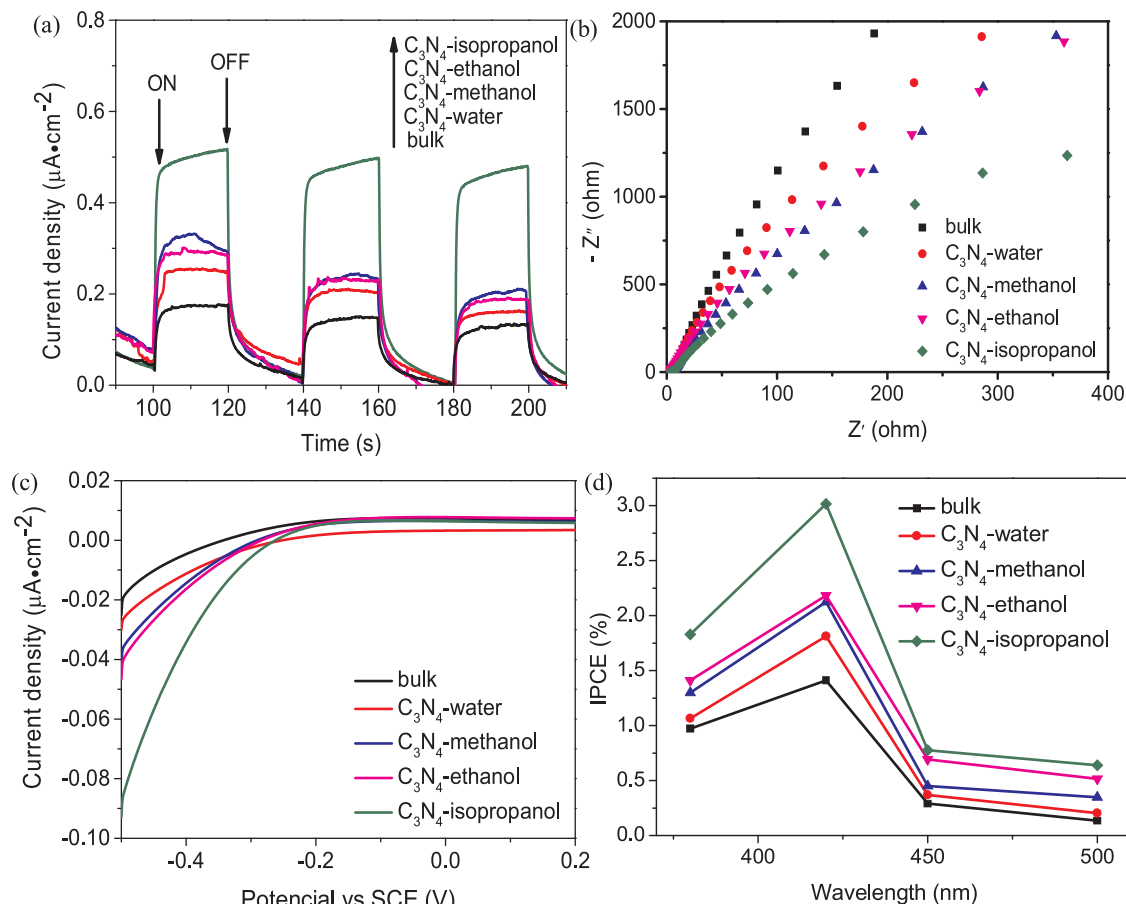


Fig. 7. Photoelectrochemical characterization of as-synthesized C₃N₄ samples. (a) The photocurrent under visible light irradiation. (b) Nyquist plots in 0.1 M Na₂SO₄ aqueous solution under visible light irradiation. (c) Current-voltage curves in 0.1 M Na₂SO₄ aqueous solution under visible light irradiation. (d) Wavelength dependence of IPCEs for bulk g-C₃N₄ and refluxed samples at different wavelength ($\lambda = 380$ nm, 420 nm, 450 nm and 500 nm) in 0.1 M Na₂SO₄ aqueous solution under visible light irradiation.

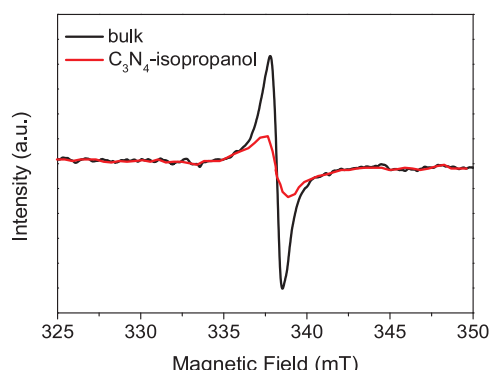


Fig. 8. EPR spectra of bulk g-C₃N₄ and C₃N₄-isopropanol samples.

The transient photocurrent of the samples was measured to evaluate the separation efficient of electron–hole pairs in the samples. The photocurrent responses of the film electrodes were prompt by the on/off of intermittent visible-light irradiation ($\lambda > 420$ nm) in 0.1 M Na₂SO₄ aqueous solution. As shown in Fig. 7a, the photocurrent response in C₃N₄-isopropanol and the synthetical samples were comparatively large with respect to that in bulk g-C₃N₄, indicating the effective separation of electron–hole pairs in C₃N₄-isopropanol. Fig. 7b shows the electrochemical impedance spectroscopy (EIS) nyquist plots of as-prepared samples under visible light irradiation ($\lambda > 420$ nm). It can be seen that the arc radius decreases in the order of bulk > C₃N₄-water > C₃N₄-methanol > C₃N₄-ethanol > C₃N₄-isopropanol, indicating less

resistance of charge across the C₃N₄-isopropanol film electrode interface and more effective separation of photogenerated electron–hole pairs and the fastest interfacial charge transfer for C₃N₄-isopropanol, which is consistent with the result of photocurrent. Fig. 7c shows the linear sweep voltammograms (LSV) and C₃N₄-isopropanol samples exhibit a cathodic shift of the onset potential from -0.3 V to -0.5 V, along with increase in the photocurrent density (-0.087 μ A cm^{-2} at -0.5 V vs. SCE.) compared with bulk C₃N₄, which is about -0.021 μ A cm^{-2} at -0.5 V vs. SCE., due to improving photoelectron transfer efficiency and reducing the charge recombination. The incident photo-to-current conversion efficiency (IPCE) was useful parameter to investigate the relationship between the photocatalytic hydrogen evolution activity and light absorption. The IPCEs spectra of as-synthesized C₃N₄ samples (Fig. 7d) match well with their absorption spectra. The maximum IPCEs are obtained at 420 nm, which are 1.41%, 1.81%, 2.12%, 2.18%, 3.02% for bulk g-C₃N₄, C₃N₄-water, C₃N₄-methanol, C₃N₄-ethanol and C₃N₄-isopropanol, respectively. Among the as-synthesized C₃N₄ samples, IPCEs of C₃N₄-isopropanol exhibit remarkable enhancement, indicating that enhanced separation efficiency of photoexcited electron–hole pairs due to its special self-assembly quasi-sphere morphology.

3.3. Reduce the internal structural defects and enhance the hydrogenation activity of photolysis water

Electron paramagnetic resonance (EPR) can be used as a sensitive and accurate method to study the unpaired electron in the sample. By the preceding XPS and PL analysis, we can conclude that the defect

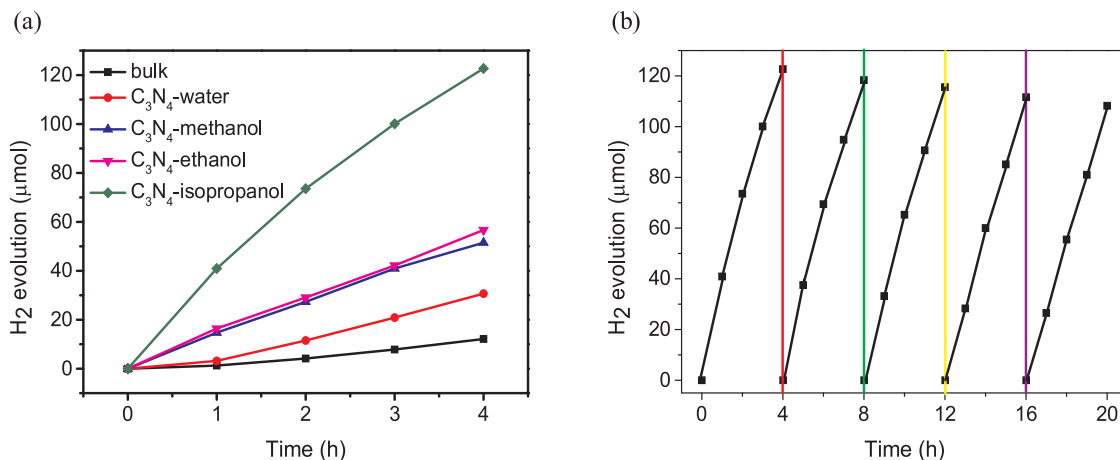


Fig. 9. (a) Photocatalytic activity test of bulk g-C₃N₄ and the refluxed samples. (b) Photocatalytic activity cycling test of C₃N₄-isopropanol sample.

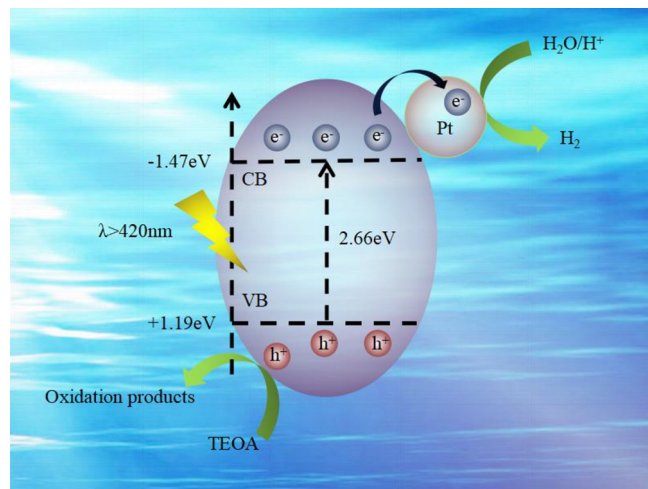


Fig. 10. Schematic illustration of photocatalytic mechanism for C₃N₄-isopropanol sample under visible light irradiation.

density of hydrogen bonding and internal structure for the C₃N₄-isopropanol sample have reduced, which can be confirmed by EPR test. The EPR test result of bulk g-C₃N₄ and C₃N₄-isopropanol is shown in Fig. 8. Both samples show a single signal, and g = 2.0048 is attached to the lone pair on the hybrid ring. As we can see, the signal strength of C₃N₄-isopropanol sample is significantly lower than that of bulk g-C₃N₄, indicating the density of lone pair electrons has decreased, suggesting that the density of internal hydrogen bond and the internal structure defect has reduced.

Hydrogen evolution reaction was carried out to evaluate the photocatalytic activity of the as-prepared samples. The photocatalytic activity was measured in a water / triethanolamine (TEOA) mixture solution under visible light irradiation. Pt (3 wt %) was used as a cocatalyst and photoloaded in situ onto the samples. As shown in Fig. 9a, the hydrogen evolution rate of C₃N₄-isopropanol (HER = 30.67 μmol h⁻¹) was much higher than that of bulk g-C₃N₄ (HER = 3.03 μmol h⁻¹). The photocatalytic stability of C₃N₄-isopropanol was examined via the photocatalytic experiments under the same reaction conditions, and no obvious deterioration was found after five cycle tests, indicating C₃N₄-isopropanol has excellent photocatalytic stability (Fig. 9b). The negligible decline of their activity may be due to consumption of sacrificial agents [53]. The comparison of photocatalytic performance for C₃N₄-isopropanol samples and some previous g-C₃N₄ photocatalysts in recent years is listed in Table S1 (Supporting Information). Although, recorded hydrogen evolution rate by us is lower than the literature reports of g-C₃N₄ samples with

ordered mesoporous structure [54], the hydrogen evolution for C₃N₄-isopropanol samples is much higher than other sphere-like g-C₃N₄ samples [55]. Furthermore, our study is valuable in the respects of modifying defects in the exfoliation of g-C₃N₄ nanosheets and showing the relationship templateless self-assembly quasi-sphere C₃N₄ samples and photocatalytic activity of hydrogen evolution performance.

The mechanism of photocatalytic reaction for water splitting is illuminated in Fig. 10. Under visible light irradiation, the C₃N₄-isopropanol samples can absorb the photons, the energy of which is higher than the intrinsic band gap of C₃N₄-isopropanol, thus the electrons can be excited and transferred from the valence band to the conduction band, meanwhile, the positive holes are left in the valence band. The excited electrons move to the Pt cocatalyst particles in situ loading on the surface of C₃N₄-isopropanol, where the H₂O/H⁺ is reduced to H₂ molecules. The photo-generated holes in the conduction band can be captured and consumed by TEOA.

The mechanism of enhanced photocatalytic activity for C₃N₄-isopropanol can be ascribed to the followed reasons: (1) g-C₃N₄ has been calcined twice, so that the condensation is more complete, and the hydrogen bonding within the structure makes the internal structure of the laminates get more orderly. (2) During the refluxed process, a little amount of C–O bonds have formed since the effect of hydroxide radical and the symmetric branched chain structure, repairing structure defect, and the formation of spherical structure has a high specific surface area, which can provide more active sites and more chance of Pt load combination, and separation efficiency of electronic-hole was enhanced. (3) The position of conduction band for C₃N₄-isopropanol is more negative than that of the bulk-C₃N₄ (Table 1), indicating it is better able to meet the conditions of the water spilling to produce hydrogenation.

4. Conclusions

In summary, self-assembly g-C₃N₄ samples without templates using the exfoliation of g-C₃N₄ nanosheets via thermal oxidation etching of bulk g-C₃N₄ as starting materials, have been successfully synthesized by a reflux method in the different organic solvent at a low temperature 65 °C. When refluxing in the solvent of isopropanol, quasi-sphere g-C₃N₄ samples have been prepared via a self-assembly process, which mostly eliminated the defects of g-C₃N₄ nanosheets, because the generation of C–O bond of g-C₃N₄ nanosheets during refluxing, bonded with hydroxyl group and the carbon chain structure of isopropanol molecule. Among all of as-synthesized samples, self-assembly quasi-sphere g-C₃N₄ particles exhibited the best photocatalytic hydrogen evolution rate and HER was 30.67 μmol h⁻¹ under visible-light irradiation, which was 10 times higher than that of bulk g-C₃N₄ (HER = 3.03 μmol h⁻¹). This highly desirable hydrogen evolution performance was attributed to quasi-sphere morphology with the elimination of surface defects and

large surface areas, which provided more active sites and enhanced charge separation efficiency. The self-assembly strategy without templates and with different polar molecular systems also provided new ideas for the synthesis of other materials.

Acknowledgements

The authors gratefully acknowledge the financial support of National Natural Science Foundation of China (Grant NO. 21777080, 21607034, 201437003 and 21621003), National Basic Research Program of China (Grant NO. 2013CB632403) and Collaborative Innovation Center for Regional Environmental Quality, Natural Science Foundation of Liaoning (Grant NO. 2015020577), Young Talents Foundation of University of Science and Technology Liaoning (Grant NO. 2015RC10, 601011507-24), the Scientific Research Foundation of the Educational Department of Liaoning Province (Grant NO. L2017122).

Appendix A. Supplementary data

Supplementary material related to this article can be found, in the online version, at doi:<https://doi.org/10.1016/j.apcatb.2018.07.017>.

References

- P. Xiong, J. Zhu, L. Zhang, X. Wang, Recent advances in graphene-based hybrid nanostructures for electrochemical energy storage, *Nanoscale Horiz.* 1 (2016) 340–374.
- R. Sahoo, A. Pal, T. Pal, 2D materials for renewable energy storage devices: outlook and challenges, *Chem. Commun.* 52 (2016) 13528–13542.
- S. Patnaik, S. Martha, G. Madras, K. Parida, The effect of sulfate pre-treatment to improve the deposition of Au-nanoparticles in a gold-modified sulfated g-C₃N₄ plasmonic photocatalyst towards visible light induced water reduction reaction, *Phys. Chem. Chem. Phys.* 18 (2016) 28502–28514.
- M. Tahir, C. Cao, F.K. Butt, F. Idrees, N. Mahmood, Z. Ali, et al., Tubular graphitic-C₃N₄: a prospective material for energy storage and green photocatalysis, *J. Mater. Chem. A* 1 (2013) 13949–13955.
- J.X. Sun, Y.P. Yuan, L.G. Qiu, X. Jiang, A.J. Xie, Y.H. Shen, et al., Fabrication of composite photocatalyst g-C₃N₄-ZnO and enhancement of photocatalytic activity under visible light, *Dalton Trans.* 41 (2012) 6756–6763.
- L. Sun, Y. Qi, C.J. Jia, Z. Jin, W. Fan, Enhanced visible-light photocatalytic activity of g-C₃N₄/Zn₂GeO₄ heterojunctions with effective interfaces based on band match, *Nanoscale* 6 (2014) 2649–2659.
- Z. Wang, W. Guan, Y. Sun, F. Dong, Y. Zhou, W.K. Ho, Water-assisted production of honeycomb-like g-C₃N₄ with ultralong carrier lifetime and outstanding photocatalytic activity, *Nanoscale* 7 (2015) 2471–2479.
- D.H. Wang, J.N. Pan, H.H. Li, J.J. Liu, Y.B. Wang, L.T. Kang, et al., A pure organic heterostructure of μ -oxo dimeric iron(III) porphyrin and graphitic-C₃N₄ for solar H₂ reduction from water, *J. Mater. Chem. A* 4 (2016) 290–296.
- M. Yang, J. Liu, X. Zhang, S. Qiao, H. Huang, Y. Liu, et al., C₃N₄-sensitized TiO₂ nanotube arrays with enhanced visible-light photoelectrochemical performance, *Phys. Chem. Chem. Phys.* 17 (2015) 17887–17893.
- Y. Wang, Z. Wang, S. Muhammad, J. He, Graphite-like C₃N₄ hybridized ZnWO₄ nanorods: synthesis and its enhanced photocatalysis in visible light, *CrystEngComm* 14 (2012) 5065–5070.
- S. Bai, X. Wang, C. Hu, M. Xie, J. Jiang, Y. Xiong, Two-dimensional g-C₍₃₎N₍₄₎: an ideal platform for examining facet selectivity of metal co-catalysts in photocatalysis, *Chem. Commun.* 50 (2014) 6094–6097.
- S. Patnaik, S. Martha, K.M. Parida, An overview of the structural, textural and morphological modulations of g-C₃N₄ towards photocatalytic hydrogen production, *RSC Adv.* 6 (2016) 46929–46951.
- M. Zhang, Y. Duan, H. Jia, F. Wang, L. Wang, Z. Su, et al., Defective graphitic carbon nitride synthesized by controllable co-polymerization with enhanced visible light photocatalytic hydrogen evolution, *Catal. Sci. Technol.* 7 (2017) 452–458.
- K.C. Christoforidis, M. Melchionna, T. Montini, D. Papoulis, E. Stathatos, S. Zafeiratos, et al., Solar and visible light photocatalytic enhancement of halloysite nanotubes/g-C₃N₄ heteroarchitectures, *RSC Adv.* 6 (2016) 86617–86626.
- P. Wu, J. Wang, J. Zhao, L. Guo, F.E. Osterloh, High alkalinity boosts visible light driven H₂ evolution activity of g-C₃N₄ in aqueous methanol, *Chem. Commun.* 50 (2014) 15521–15524.
- Y. Zheng, X. Dou, H. Li, J.-M. Lin, Bisulfite induced chemiluminescence of g-C₃N₄nanosheets and enhanced by metal ions, *Nanoscale* 8 (2016) 4933–4937.
- Y. Jiang, S. Guo, R. Hao, Y. Luan, Y. Huang, F. Wu, et al., A hybridized heterojunction structure between TiO₂ nanorods and exfoliated graphitic carbon-nitride sheets for hydrogen evolution under visible light, *CrystEngComm* 18 (2016) 6875–6880.
- Y. Liu, X. Zhang, J. Wang, P. Yang, In situ growth of sulfide/g-C₃N₄ nano-heterostructures with an adjusted band gap toward enhanced visible photocatalysis, *Phys. Chem. Chem. Phys.* 18 (2016) 31513–31520.
- D. Chen, K. Wang, T. Ren, H. Ding, Y. Zhu, Synthesis and characterization of the ZnO/mpg-C₍₃₎N₍₄₎ heterojunction photocatalyst with enhanced visible light photoactivity, *Dalton Trans.* 43 (2014) 13105–13114.
- Y. Wang, X. Bai, C. Pan, J. He, Y. Zhu, Enhancement of photocatalytic activity of Bi₂WO₆ hybridized with graphite-like C₃N₄, *J. Mater. Chem.* 22 (2012) 11568–11573.
- L. Sun, X. Zhao, C.-J. Jia, Y. Zhou, X. Cheng, P. Li, et al., Enhanced visible-light photocatalytic activity of g-C₃N₄-ZnWO₄ by fabricating a heterojunction: investigation based on experimental and theoretical studies, *J. Mater. Chem.* 22 (2012) 23428–23438.
- J. Wang, Z. Guan, J. Huang, Q. Li, J. Yang, Enhanced photocatalytic mechanism for the hybrid g-C₃N₄/MoS₂ nanocomposite, *J. Mater. Chem. A* (2014) 7960–7966.
- L.-R. Zou, G.-F. Huang, D.-F. Li, J.-H. Liu, A.-L. Pan, W.-Q. Huang, A facile and rapid route for synthesis of g-C₃N₄ nanosheets with high adsorption capacity and photocatalytic activity, *RSC Adv.* 6 (2016) 86688–86694.
- X. Bu, Y. Bu, S. Yang, F. Sun, L. Tian, Z. Peng, et al., Graphitic carbon nitride nanoribbon for enhanced visible-light photocatalytic H₂ production, *RSC Adv.* 6 (2016) 112210–112214.
- P. Xia, B. Zhu, J. Yu, S. Cao, M. Jaroniec, Ultra-thin nanosheet assemblies of graphitic carbon nitride for enhanced photocatalytic CO₂ reduction, *J. Mater. Chem. A* 5 (2017) 3230–3238.
- J. Cheng, H. Zhao, K. Lv, X. Wu, Q. Li, Y. Li, X. Li, J. Sun, Drastic promoting the visible photoreactivity of layered carbon nitride by polymerization of dicyandiamide at high pressure, *Appl. Catal. B* 232 (2018) 330–339.
- J. Hong, C. Chen, F.E. Bedoya, G.H. Kelsall, D. O'Hare, C. Petit, Carbon nitride nanosheet-metal-organic framework nanocomposites with synergistic photocatalytic activities, *Catal. Sci. Technol.* 6 (2016) 5042–5051.
- C. Han, Y. Lu, J. Zhang, L. Ge, Y. Li, C. Chen, et al., Novel PtCo alloy nanoparticle decorated 2D g-C₃N₄ nanosheets with enhanced photocatalytic activity for H₂ evolution under visible light irradiation, *J. Mater. Chem. A* 3 (2015) 23274–23282.
- Z. Huang, F. Li, B. Chen, G. Yuan, Nanosheets of graphitic carbon nitride as metal-free environmental photocatalysts, *Catal. Sci. Technol.* 4 (2014) 4258–4264.
- J. Xu, H.T. Wu, X. Wang, B. Xue, Y.X. Li, Y. Cao, A new and environmentally benign precursor for the synthesis of mesoporous g-C₃N₄ with tunable surface area, *Phys. Chem. Chem. Phys.* 15 (2013) 4510–4517.
- H. Zhao, H. Yu, X. Quan, S. Chen, H. Zhao, H. Wang, Atomic single layer graphitic-C₃N₄: fabrication and its high photocatalytic performance under visible light irradiation, *RSC Adv.* 4 (2014) 624–628.
- M.Z. Rahman, J. Ran, Y. Tang, M. Jaroniec, S.Z. Qiao, Surface activated carbon nitride nanosheets with optimized electro-optical properties for highly efficient photocatalytic hydrogen production, *J. Mater. Chem. A* 4 (2016) 2445–2452.
- W. Wang, J.C. Yu, Z. Shen, D.K. Chan, T. Gu, g-C₃N₄ quantum dots: direct synthesis, upconversion properties and photocatalytic application, *Chem. Commun.* 50 (2014) 10148–10150.
- F. Cheng, H. Wang, X. Dong, The amphoteric properties of g-C₃N₄ nanosheets and fabrication of their relevant heterostructure photocatalysts by an electrostatic reassembly route, *Chem. Commun.* 51 (2015) 7176–7179.
- L. Bi, D. Xu, L. Zhang, Y. Lin, D. Wang, T. Xie, Metal Ni-loaded g-C₃N₄ for enhanced photocatalytic H₂ evolution activity: the change in surface band bending, *Phys. Chem. Chem. Phys.* 17 (2015) 29899–29905.
- F. He, G. Chen, Y. Yu, Y. Zhou, Y. Zheng, S. Hao, The synthesis of condensed C-PDA-g-C₃N₄ composites with superior photocatalytic performance, *Chem. Commun.* 51 (2015) 6824–6827.
- P. Niu, L. Zhang, G. Liu, H.-M. Cheng, Graphene-like carbon nitride nanosheets for improved photocatalytic activities, *Adv. Funct. Mater.* 22 (2012) 4763–4770.
- W. Che, Cheng W, T. Yao, F. Tang, W. Liu, H. Su, Y. Huang, Q. Liu, J. Liu, F. Hu, Z. Pan, Z. Sun, S. Wei, Fast photoelectron transfer in (C_{ring})-C₃N₄ plane heterostructural nanosheets for overall water splitting, *J. Am. Chem. Soc.* 139 (2017) 2012–3026.
- W.J. Ong, L.L. Tan, S.P. Chai, S.T. Yong, Heterojunction engineering of graphitic carbon nitride (g-C₃N₄) via Pt loading with improved daylight-induced photocatalytic reduction of carbon dioxide to methane, *Dalton Trans.* 44 (2015) 1249–1257.
- Y. Cao, Z. Zhang, J. Long, J. Liang, H. Lin, H. Lin, et al., Vacuum heat-treatment of carbon nitride for enhancing photocatalytic hydrogen evolution, *J. Mater. Chem. A* 2 (2014) 17797–17807.
- M. Tahir, C. Cao, F.K. Butt, S. Butt, F. Idrees, Z. Ali, et al., Large scale production of novel g-C₃N₄ micro strings with high surface area and versatile photodegradation ability, *CrystEngComm* 16 (2014) 1825–1830.
- Y. Li, H. Xu, S. Ouyang, D. Lu, X. Wang, D. Wang, et al., In situ surface alkalinized g-C₃N₄ward enhancement of photocatalytic H₂evolution under visible-light irradiation, *J. Mater. Chem. A* 4 (2016) 2943–2950.
- D. Jiang, L. Chen, J. Zhu, M. Chen, W. Shi, J. Xie, Novel p-n heterojunction photocatalyst constructed by porous graphite-like C₃N₄ and nanostructured BiOI: facile synthesis and enhanced photocatalytic activity, *Dalton Trans.* 42 (2013) 15726–15734.
- F. Ding, D. Yang, Z. Tong, Y. Nan, Y. Wang, X. Zou, et al., Graphitic carbon nitride-based nanocomposites as visible-light driven photocatalysts for environmental purification, *Environ. Sci.: Nano* 4 (2017) 1455–1469.
- H. Ou, L. Lin, Y. Zheng, P. Yang, Y. Fang, X. Wang, Tri-s-triazine-based crystalline carbon nitride nanosheets for an improved hydrogen evolution, *Adv. Mater.* 29 (2017) 1700008.
- X.H. Song, L. Feng, S.L. Deng, S.Y. Xie, L.S. Zheng, Simultaneous exfoliation and modification of graphitic carbon nitride nanosheets, *Adv. Mater. Interfaces* 4 (2017)

1700339.

- [47] X. Bai, S. Yan, J. Wang, L. Wang, W. Jiang, S. Wu, et al., A simple and efficient strategy for the synthesis of a chemically tailored g-C₃N₄ material, *J. Mater. Chem. A* 2 (2014) 17521–17529.
- [48] X. Zhang, X. Xie, H. Wang, J. Zhang, B. Pan, Y. Xie, Enhanced photoresponsive ultrathin graphitic-phase C₃N₄ nanosheets for bioimaging, *J. Am. Chem. Soc.* 135 (2012) 18–21.
- [49] Y. Huang, Y. Wang, Y. Bi, J. Jin, M.F. Ehsan, M. Fu, et al., Preparation of 2D hydroxyl-rich carbon nitride nanosheets for photocatalytic reduction of CO₂, *RSC Adv.* 5 (2015) 33254–33261.
- [50] Y. Xu, M. Xie, S. Huang, H. Xu, H. Ji, J. Xia, et al., High yield synthesis of nano-size g-C₃N₄ derivatives by a dissolve-regrowth method with enhanced photocatalytic ability, *RSC Adv.* 5 (2015) 26281–26290.
- [51] P. Wu, J. Wang, J. Zhao, L. Guo, F.E. Osterloh, Structure defects in g-C₃N₄ limit visible light driven hydrogen evolution and photovoltage, *J. Mater. Chem. A* 2 (2014) 20338–20344.
- [52] X. Bai, L. Wang, R. Zong, Y. Zhu, Photocatalytic activity enhanced via g-C₃N₄ nanoplates to nanorods, *J. Phys. Chem. C* 117 (2013) 9952–9961.
- [53] Z. Wu, C. Gong, J. Yu, L. Sun, W. Xiao, C. Lin, Enhanced visible light photoelectrocatalytic activity over Cu_xZn_{1-x}In₂S₄@TiO₂ nanotube array hetero-structures, *J. Mater. Chem. A* 5 (2017) 1292–1299.
- [54] X. Chen, Y.-S. Jun, K. Takanabe, K. Maeda, K. Domen, X. Fu, M. Antonietti, X. Wang, Ordered mesoporous SBA-15 type graphitic carbon nitride: a semiconductor host structure for photocatalytic hydrogen evolution with visible light, *Chem. Mater.* 21 (2009) 4093–4095.
- [55] Q. Gu, Y. Liao, L. Yin, J. Long, X. Wang, C. Xue, Template-free synthesis of porous graphitic carbon nitride microspheres for enhanced photocatalytic hydrogen generation with high stability, *Appl. Catal., B* 165 (2015) 503–510.